Journal of Power Sources 195 (2010) 5005–5012

Contents lists available at ScienceDirect

Journal of Power Sources

journal homepage: www.elsevier.com/locate/jpowsour

A new solid-state process for synthesis of $LiMn_{1.5}Ni_{0.5}O_{4-\delta}$ spinel

Nader Marandian Hagh*, Glenn G. Amatucci

Energy Storage Research Group, Department of Materials Science and Engineering, Rutgers The State University of New Jersey, 671 US Highway 1, North Brunswick, NJ 08902, USA

ARTICLE INFO

Article history:
Received 24 December 2009
Received in revised form 4 February 2010
Accepted 4 February 2010
Available online 11 February 2010

Keywords:
Spinel
High voltage cathode
Nickel manganese oxide
Solid-state synthesis
Lithiation

ABSTRACT

A new two-step solid-state process was developed for synthesis of a pure phase 4.7 V $LiMn_{1.5}Ni_{0.5}O_{4-\delta}$ (LMNO) spinel of good electrochemical properties. This process which was based on formation of stable $Ni_{1-x}Mn_2O_{4-\delta}$ ($x \leq 0.33$) spinel followed by subsequent lithiation, demonstrated the emerging of $LiMn_{1.5}Ni_{0.5}O_{4-\delta}$ frame work at temperatures of as low as 350 °C. During this lithiation process, migration of metal ions (Ni/Mn) from partially occupied tetrahedral 8a sites (in $Ni_{0.67}Mn_2O_{4-\delta}$) toward octahedral 16d site occurred. The resultant spinel material displayed low irreversible loss, a 97% columbic efficiency and 6% loss in discharge capacity after 100 cycles at 60 °C.

1. Introduction

The current trend of high cost fossil-type fuels along with environmental issues of global warming signal the urgency of alternative energy sources such as wind, solar or electrochemical energy storage systems. Among the various available energy storage systems, secondary Li-ion batteries with their highest power and energy densities have been enlisted for a wide variety of applications ranging from consumer electronics and automotive to biomedical and aerospace applications.

Besides the key issues of cost, safety, reliability and being environmentally benign, battery materials must satisfy the required power/energy density. Among the Li-ion battery systems with high voltage cathodes, 3D Li intercalation/de-intercalation network of $Li_{1-x}Mn_{2-y}M_yO_4$ (M: Ni, Fe, Cr, Co, Cu, Mo) [1–10] as a derivative of $LiMn_2O_4$ spinel [11] has been an attractive candidate. The increased voltage from 4 V to ~4.7 (versus Li/Li^+) of Ni-doped spinel relative to the parent $LiMn_2O_4$ spinel by partial substitution of Mn for Ni has generated particular interest. Indeed, this spinel provides a typical capacity $\geq$135 mAh g^{-1} ($\geq$92% of theoretical value) and practical gravimetric and volumetric energy densities of $\geq$635 Wh kg^{-1} and 2820 Wh l^{-1}, respectively.

The direct relationship between property and processing is generally applicable for the broad spectrum of functional materials including those in the electrochemical energy storage systems. The electrochemical properties of the cell determined by the crystal structure, morphology, and stoichiometry of the active material are directly influenced by the type of synthesis route. Wet chemical synthesis techniques such as sol–gel or Pechini have the advantage of metal-ion mixing in atomic scale thereby providing homogenous composition, narrow particle size distribution and highly reactive powder which require lower crystallization/annealing temperature than conventional solid-state process. These high surface area particles with nano-size morphology provide high rate due to larger cathode–electrolyte interface for Li insertion/extraction and shorter Li^+ diffusion path in the bulk. However, large electrode–electrolyte interface area promotes electrolyte side reactions and adversely affects the long term cycling stability of the cell. In addition, the high cost of the fabrication process due to complex synthesis routes, expensive precursors, and various gaseous reaction products, makes the sol–gel/solution based process not cost efficient in the context of large scale synthesis. Regarding the current energy needs and practical challenges in satisfying the requirements of high rate and high capacity in large scale synthesis of pure crystalline cathode material, it is necessary to develop a facile synthesis process which satisfies these requirements without sacrificing the electrochemical properties.

Typical inexpensive solid-state process has always been attractive despite of lower homogeneity and higher annealing temperatures relative to many solution based methods. In the case of $LiMn_{1.5}Ni_{0.5}O_4$, the higher temperature of reaction and lack of atomic mixing promotes second phase formation (such as NiO or $Li_{1-x}Ni_xO_2$), accelerates evaporation of volatile components (such as Li) and produces non-stoichiometric spinels. The difficulty in synthesizing pure, single phase $LiMn_{1.5}Ni_{0.5}O_4$ through solid-state

* Corresponding author. Present Address: NEI Corporation, 400E Apgar Drive, Somerset NJ 08873, USA. Tel.: +1 732 868 3141; fax: +1 732 868 3143.
E-mail address: nmhagh@neicorporation.com (N.M. Hagh).

0378-7753/$ – see front matter © 2010 Elsevier B.V. All rights reserved.
doi:10.1016/j.jpowsour.2010.02.011

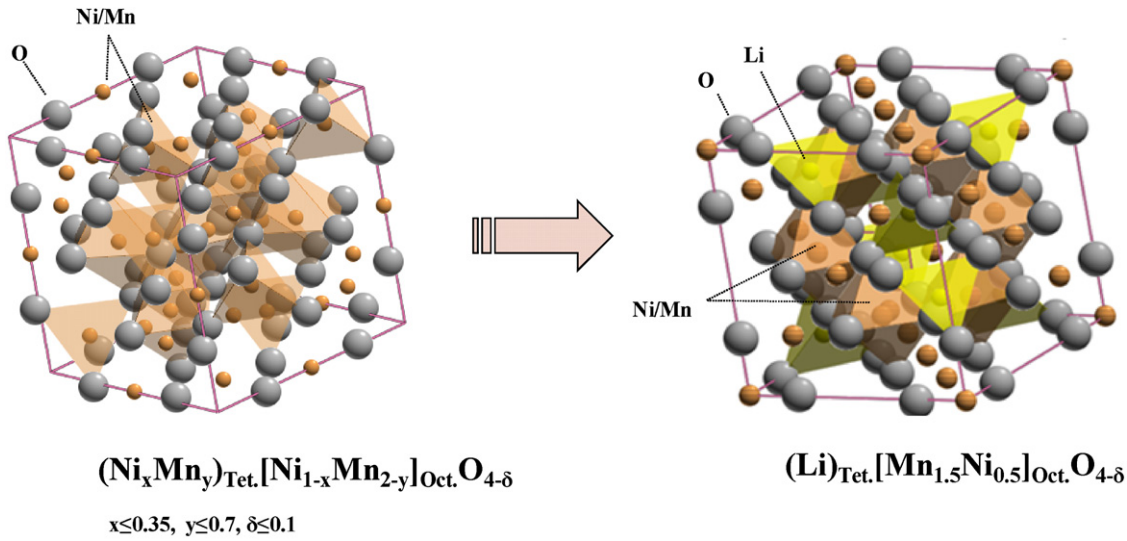

Fig. 1. Schematic representation of new solid state process through $(Ni_xMn_y)_{Tet.}(Ni_{1-x}Mn_{2-y})_{Oct.}O_{4-\delta}$ transformation to $(Li)_{Tet.}(Mn_{1.5}Ni_{0.5})_{Oct.}O_{4-\delta}$ spinel during lithiation process ($x \leq 0.35$, $y \leq 0.7$, $\delta \leq 0.1$).

process was reported by others [1,12,13] where the formation of non-stoichiometric spinel along with second phase(s) as inactive material(s) deteriorated the electrochemical properties. It is believed that the higher reactivity of Li precursors relative to Ni or Mn oxides at low temperatures prevents single phase formation of spinel from oxide-based precursors. In order to prevent this selective reaction process caused by Li, we carried out our solid-state process in two steps.

Our new two-step process is analogous to the "Columbite" method for the synthesis of piezoelectric ceramic powder, $Pb(Mg_{1/3}Nb_{2/3})O_3$ (PMN), from the ternary system of $PbO–Nb_2O_5–MgO$ [14,15] where the high affinity of PbO to react with Nb_2O_5 lead to a formation of unfavorable pyrochlore compounds (i.e. $Pb_2Nb_2O_7$, $Pb_3Nb_4O_{13}$). In this regard, the role of PbO in piezoelectric system of $PbO–Nb_2O_5–MgO$ is analogous to Li_2O in ternary system of $Li_2O–NiO–MnO_2$. In fact, our selection of the two-step process was based on high reactivity of Li with NiO which thermodynamically is in favor of $Li_xNi_xO_2$ formation along with formation of $LiMn_{1.5}Ni_{0.5}O_4$ phase and is routinely seen as a second phase in traditional solid-state synthesis.

In this paper, we report on the new two-step solid-state process for synthesis of $LiMn_{1.5}Ni_{0.5}O_4$ spinel and reported the physical and electrochemical properties. The solid-state synthesis of $LiMn_{1.5}Ni_{0.5}O_4$ spinel was achieved in two separate steps. First, less reactive components of NiO and MnO_2 were annealed to form pure $Ni_{1-x}Mn_2O_4$ ($x \leq 0.33$) spinel. The spinel phase is in the proper stoichiometry and crystal type as opposed to the more common $NiMnO_3$ ilmenite. Lithiation is then accomplished by reaction of the $Ni_{0.67}Mn_2O_4$ spinel with a Li compound such as Li_2CO_3 to form the final $LiMn_{1.5}Ni_{0.5}O_4$ spinel composition. Fig. 1 demonstrates the $(Ni_{x+z}Mn_y)_{Tet.}(Ni_{1-x-z}Mn_{2-y})_{Oct.}O_{4-\delta}$ transformation into the $(Li)_{Tet.}(Mn_{1.5}Ni_{0.5})_{Oct.}O_{4-\delta}$ spinel during lithiation process. During this process, the residing metal ions at tetrahedral sites (such as Ni and Mn) are moved toward adjacent octahedral positions in the crystal structure. Developing this process allowed us to initiate the spinel formation starting as low as 350 °C.

2. Experimental

$LiMn_{1.5}Ni_{0.5}O_{4-\delta}$ spinels were prepared by conventional two-step solid-state process. First, the stoichiometric amounts of NiO (Sigma–Aldrich, 99.8%) and MnO_2 (Broken Hill Proprietary's [BHP] Australian EMD) were thoroughly mixed using zirconia milling media and anhydrous acetone followed by drying at 110 °C. The dried powder was heat treated at annealing temperatures of 600–900 °C for 3 h to form pure $Ni_{0.67}Mn_2O_4$ spinel. The appropriate moles of Li_2CO_3 were mixed with pure synthesized $Ni_{0.67}Mn_2O_4$ powder through a similar wet ball milling procedure. After drying the mixture at 110 °C, the powder was heat treated at annealing temperature of 350–900 °C for 12 h. For studying the effect of surface area and comparison with solid-state process, nano-powder $LiMn_{1.5}Ni_{0.5}O_4$ spinel was also synthesized through Pechini process. The details of this wet chemical based process are explained elsewhere [16].

2032 coin type stainless steel and Al plated stainless steel cells were utilized for electrochemical characterization. Each cell consisted of the positive electrode spinel material, negative electrode (Li metal) and electrolyte, 1 M $LiPF_6$ dissolved in mixture of ethylene carbonate–dimethyl carbonate (EC-DMC). The positive electrode tape was prepared through the tape casting of 52 wt% active spinel cathode material, 13 wt% Super P, and 35 wt% PVDF-HFP (Polyvinylidine fluoride hexafluoro propylene) binder with DBP (Dibutyl Phthalate) as a plasticizer. The plasticizer was extracted from the electrode prior to use by successive extractions in anhydrous dimethyl ether. The relatively low active content is utilized to be sure that the electrode formulation is not the limiting factor in the electrochemistry of the materials. Our intent is not to show data that has failure induced by the breakdown of the percolation network/binder in the electrode versus phenomena associated with the material itself. The prepared cathode tape was assembled in He-filled glove box and cycled using the Maccor Galvanostat cycler. The charge–discharge cycling of the cells was achieved between 3.5 and 5.0 V at the cycling rates of 44 mA g^{-1}.

The morphology of the powders was studied by field emission scanning electron microscopy (FESEM; LEO (ZEISS) 982) with electron low accelerating voltage of 5.0 kV. Energy Dispersive Spectroscopy (EDS) of the powders was also studied by LEO (ZEISS) 982 PGT with the accelerating voltages of 5 and 10 kV. A Scintag X-ray diffractometer with Cu K_α radiation (40 kV, 35 mA) was utilized to characterize the phase and lattice parameter of the synthesized powders. For lattice constant measurements, internal standard (silicon) was used to correct the system error. The multipoint Brunauer–Emmett–Teller (BET) surface area was measured by a Micromeritics ASAP 2010 surface area analyzer. For Fourier transformed infrared (FTIR) study, a Thermonicolet Avatar 36 was used. The sample preparation for FTIR was carried out by diluting

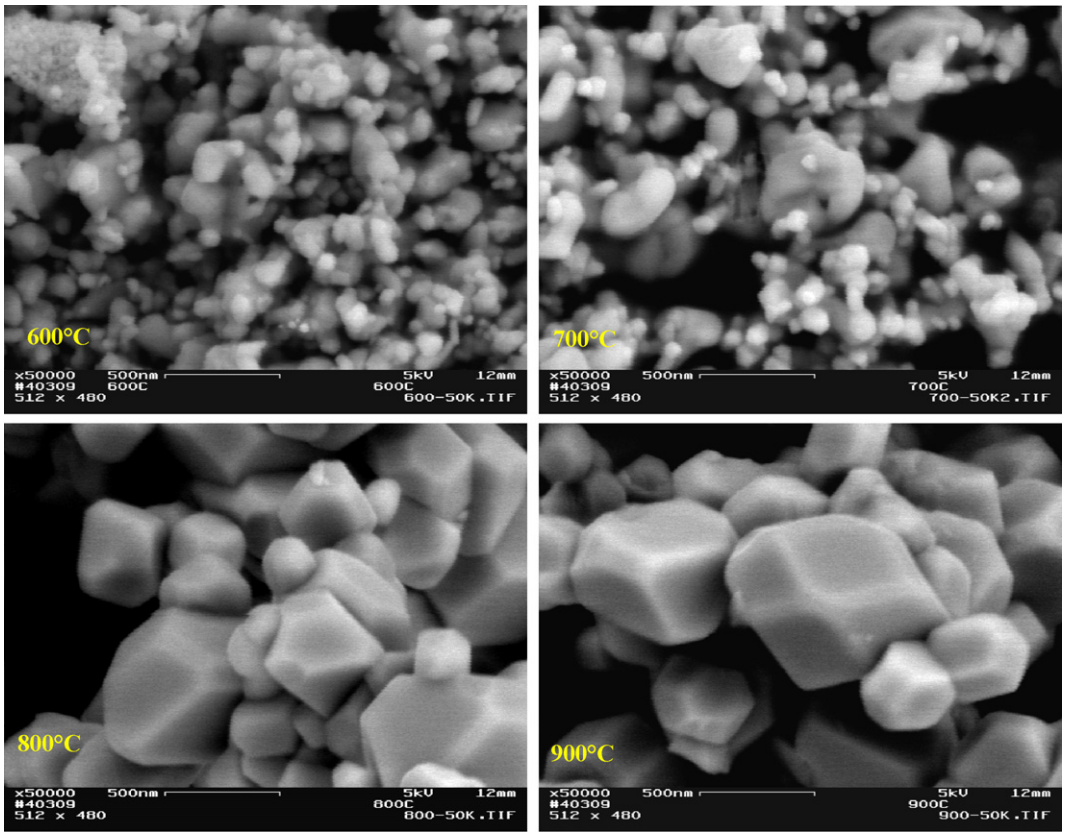

Fig. 2. SEM micrographs of $Ni_{1-x}Mn_2O_4$ ($x \leq 0.33$) spinel formation at different annealing temperatures.

a small amount of powder in 100 mg of KBr powder. Collection of IR data was based on average 100 scans taken between 4000 and 400 cm^{-1} with selected resolution of 4 cm^{-1}.

3. Results and discussions

3.1. Solid-state synthesis of spinel

The FESEM study was performed to obtain the particle characteristics (such as morphology and particle size) of the precursor in which the spinel was templated upon. The FESEM micrographs of the NiO and MnO_2 mixture heat treated at temperature range of 600–900 °C are shown in Fig. 2. At temperatures below 700 °C, particles of two distinct particle size distributions are shown which suggest the presence of multiple phases with irregular morphologies. Above 700 °C, seemingly single phase, well-faceted crystallized spinel particles of 200–700 nm were observed.

Phase analysis of the heat treated materials by XRD is shown in Fig. 3. The reaction between NiO and MnO_2 at $T \leq 700$ °C formed

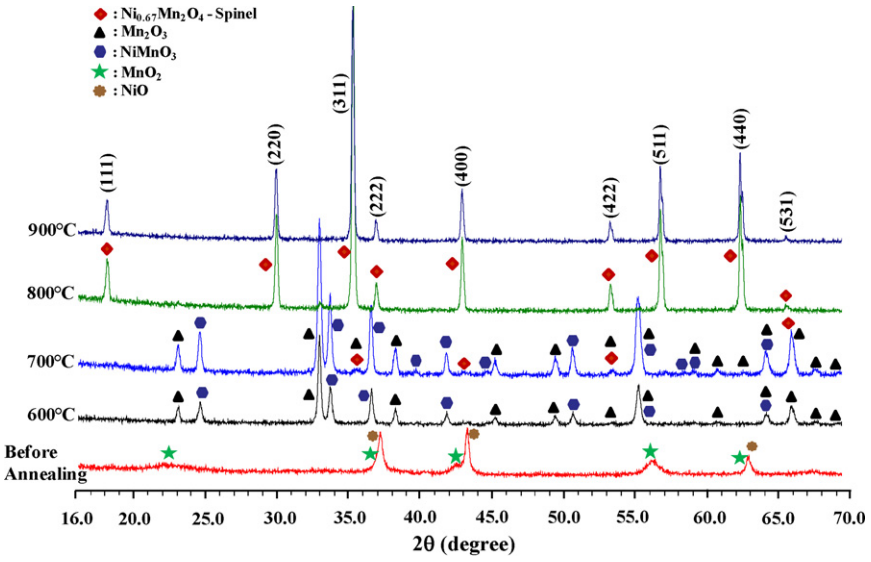

Fig. 3. Effect of annealing temperature on the formation of nickel manganese oxide spinel ($Ni_{1-x}Mn_2O_4$; $x \leq 0.33$). Dwell time: 3 h in air atmosphere.

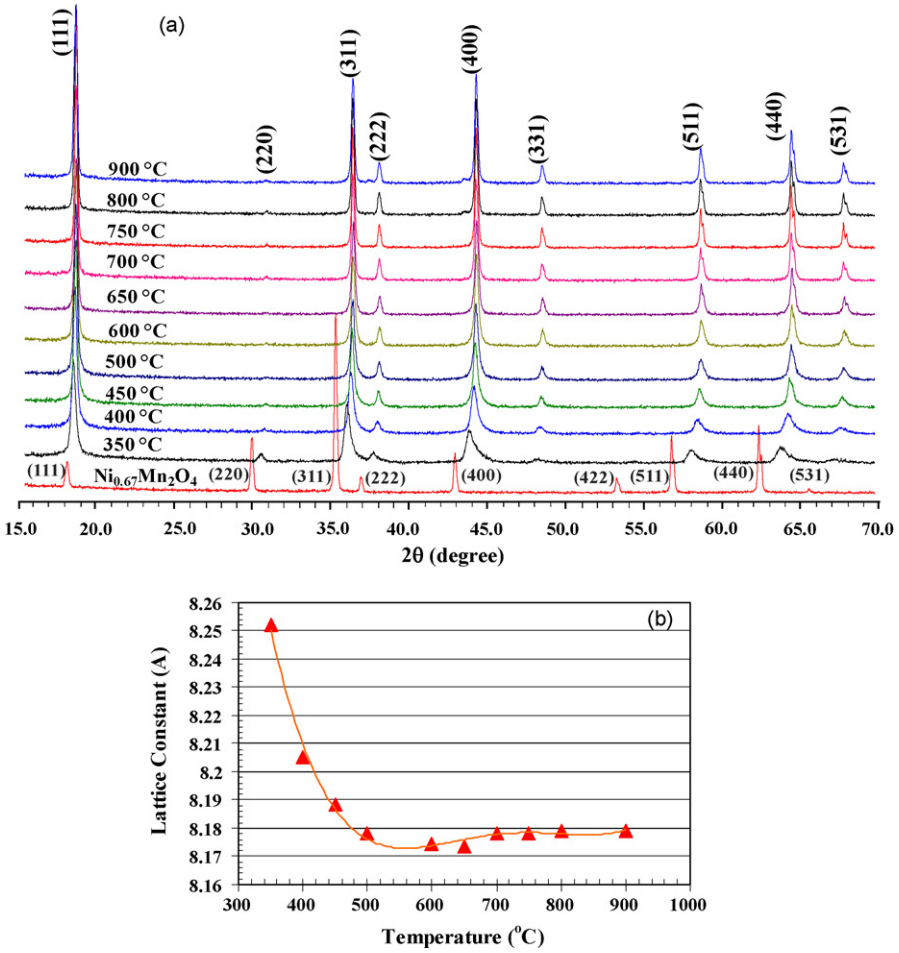

Fig. 4. (a) X-ray diffraction patterns of $LiMn_{1.5}Ni_{0.5}O_4$ spinel formation by incorporating Li_2CO_3 into $Ni_{1-x}Mn_2O_4$ ($x \leq 0.33$) structure at different annealing temperatures, and (b) change in corresponding lattice parameter of final spinel.

the intermediate compounds of $NiMnO_3$ with ilmenite structure (rhombohedral; $R\bar{3}$) and cubic Mn_2O_3 ($Ia\bar{3}$) as major phases along with minor traces of cubic spinel $Ni_{0.67}Mn_2O_4$ ($Fd\bar{3}m$). The multiple phases are consistent with the FESEM results of Fig. 2 which the prominence of cubic spinel was increased with increasing temperatures. At $700\,^{\circ}C < T \leq 800\,^{\circ}C$, reaction among ilmenite $NiMnO_3$ and cubic Mn_2O_3 phases lead to an increase in spinel phase ($Ni_{0.67}Mn_2O_4$) and a pure phase $Ni_{0.67}Mn_2O_4$ spinel was observed at temperatures >800 °C consistent with the FESEM results. These results are in good agreement with $Ni_{1-x}Mn_2O_4$ ($x = 0$) composition (similar to our composition $Ni_{1-x}Mn_2O_4$; $x = 0.33$, but with higher Ni content) reported by Wickham [17] and Tang et al. [18]. The $Ni_{1-x}Mn_2O_4$ ($x \geq 0$) is an inverse spinel with the distinctive metal-ion distribution which makes it attractive as NTC (Negative Temperature Coefficient) material for thermistor applications [19]. Cation distribution in $NiMn_2O_4$ spinel reported by Tang [18], Macklen [20] and Legros [21] showing (1) both Ni and Mn ions occupy tetrahedral and octahedral sites in an inverse spinel structure and (2) the Ni^{2+} ion has strong affinity to reside at octahedral sites which induces the valence change in Mn^{3+} to Mn^{4+}. This valence change plays a key role in the high conductivity of $NiMn_2O_4$. The proposed high temperature cation distribution of this spinel above 750 °C was $(Ni^{2+}{}_{1-x}Mn^{2+}{}_x)_{Tet.}(Ni^{2+}{}_xMn^{3+}{}_{2-2x}Mn^{4+}{}_x)_{Oct.}O_4$ where x is the degree of inversion (inversely proportional with annealing temperature) depending on the method of powder's preparation [18]. More specific cation distribution for spinel annealed at 900 °C was similarly reported by Macklen [20] and Legros [21] proposing the chemical formula of $(Ni^{2+}{}_{0.35}Mn^{2+}{}_{0.65})_{Tet.}(Ni^{2+}{}_{0.65}Mn^{3+}{}_{0.70}Mn^{4+}{}_{0.65})_{Oct.}O_4$ and $(Ni^{2+}{}_{0.30}Mn^{2+}{}_{0.70})_{Tet.}(Ni^{2+}{}_{0.70}Mn^{3+}{}_{0.60}Mn^{4+}{}_{0.70})_{Oct.}O_4$, respectively. The report of cation mixing on the tetrahedral site and the presence of Mn^{2+} can be similarly speculated to be present in our studied composition ($Ni_{1-x}Mn_2O_4$; $x = 0.33$).

The final composition of $LiMn_{1.5}Ni_{0.5}O_{4-\delta}$ spinel was formed by the reaction of Li_2CO_3 with $Ni_{0.67}Mn_2O_{4-\delta}$ which was annealed at 900 °C. The X-ray diffraction pattern of $LiMn_{1.5}Ni_{0.5}O_{4-\delta}$ spinels heat treated at temperature range of 350–900 °C is illustrated in Fig. 4a and b. As shown, the transformation of the $Ni_{0.67}Mn_2O_{4-\delta}$ ($a = 8.4314$ Å) to $LiMn_{1.5}Ni_{0.5}O_{4-\delta}$ spinel ($a = 3.2506$ Å) at $T = 350\,^{\circ}C$ occurred upon Li introduction. Although the two phases are isomorphic, the formation of the lithiated phase is accompanied by a reduction in the volume of the unit cell and the weakening of the intensity of the (2 2 0) and (4 2 2) Bragg reflections. The latter is consistent with the replacement of an 8a tetrahedral site occupied by transition metals of high scattering factor relative to that of an 8a tetrahedral site with Li which has a scattering factor approximately 10× lower. Lithium introduction into the $Ni_{0.67}Mn_2O_{4-\delta}$ structure, while diminishing the (2 2 0) and (4 2 2) peak intensities, paralleled a growth in the peak intensity of the (1 1 1) plane. This is consistent with the Ni/Mn move to the (1 1 1) planes where the metal ions typically reside in the ordered ($P4_332$) and disordered ($Fd\bar{3}m$) $LiMn_{1.5}Ni_{0.5}O_{4-\delta}$ spinel. This growing intensity ratio of (1 1 1)/(2 2 0) was observed up to 500 °C as shown in Fig. 5. At annealing temperatures higher than 500 °C the intensity ratio approached a plateau representing a decrease in metal-ion migra-

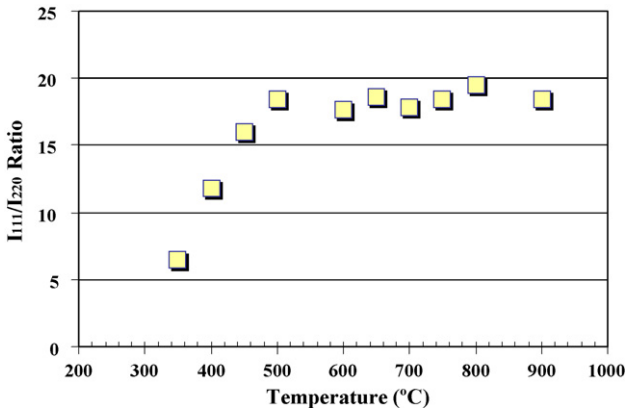

Fig. 5. Representation of cation ordering by changing the I_{111}/I_{220} relative intensity ratio at different annealing temperatures ranging from 350 to 900 °C.

tion. The detection of the minor traces of nickel rich composition such as Ni_6MnO_8 and $Li_xNi_{1-x}O_2$ as a second phase occurred at higher annealing temperatures ($T \geq 800$ °C), where the severe oxygen and lithium loss disintegrated the spinel structure.

The effect of annealing temperature on the lattice parameter of the two-step SS process is illustrated in Fig. 4b. The sharp decrease up to 650 °C followed by slight increase up to 900 °C can be explained by the temperature induced variation in Mn oxidation state. As reported by Zhong et al. [1], the average Mn oxidation state in $LiMn_{1.5}Ni_{0.5}O_4$ spinel prepared by sol–gel increased to 3.97 when the annealing temperature reached approximately 600 °C. This was found to correspond to a decrease in the lattice parameter as is shown similarly in our solid-state process at a slightly higher temperature of 650 °C. The 50 °C temperature difference observed in our process may be explained by the lower surface area of current macro-size spinel relative to high reactive nano-size particles obtained through sol–gel process in Zhong's report. At higher temperatures ($T \geq 650$ °C), reduction in Mn valence (Mn^{4+} to the larger Mn^{3+}) is responsible for expansion of the crystal structure. This reduction is induced by oxygen loss with the possible formation of nickelate secondary phase [16].

3.2. FTIR of the annealed samples

Metal-ion ordering in the octahedral sites of the $(Li)[Mn_{1.5}Ni_{0.5}]O_4$ spinel results in the assignment to either a space group of $P4_332$ (ordered) or $Fd\bar{3}m$ (disordered transition metal). The former represents the Mn and Ni ordering in 12d and 4b sites, while the latter indicates the randomly occupation of Ni/Mn in 16d site of octahedral. Identification of cation ordering by X-ray diffraction is difficult to achieve except in high resolution X-ray diffraction or neutron diffraction due to a very weak diffraction peaks of superlattice lines of (1 1 0), (2 1 0), (3 1 0) in the ordered spinel [22,23]. FTIR is an alternative and quick technique which can qualitatively determine the cation ordering.

Fig. 6 illustrates the FTIR graphs of the $LiMn_{1.5}Ni_{0.5}O_{4-\delta}$ spinels annealed in the temperature range of 350–900 °C. The Mn–O and Ni–O bands at 628 and 509 cm^{-1} developed in the sample which was annealed at 350 °C. Increase in annealing temperature developed the second peak of Mn–O band at 557 cm^{-1} which reached to a maximum intensity at 600 °C and diminished with a further increase in annealing temperature. Besides the Mn–O bands, there are two distinctive Ni–O bands for powders annealed at 600 °C located at 595 and 509 cm^{-1}. It has been shown that the distinctive peaks located at 557 cm^{-1} and also 595 cm^{-1} are fingerprints of metal-ion ordering. Similar metal-ion-oxygen bands were observed in solid-state processed spinel reported by Ariyoshi

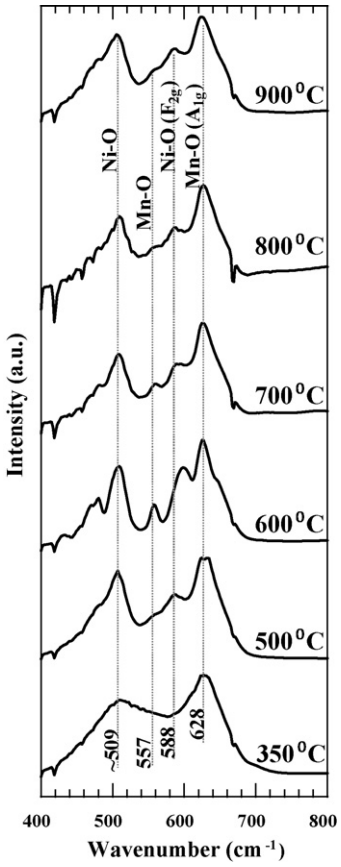

Fig. 6. FTIR spectra of $LiMn_{1.5}Ni_{0.5}O_4$ spinels prepared through the two-step process at different annealing temperatures.

et al. [22] and Pechini-processed spinel reported by Kunduraci et al. [16,24]. After mixing at 600 °C, the ordering related peak at 557 cm^{-1} gradually reduced with annealing temperatures indicating that the materials developed random metal-ion distribution in octahedral sites ($Fd\bar{3}m$). This has been previously linked to the gradual loss of oxygen and the subsequent formation of the large Mn^{3+} ions which disturbed the delicate energy advantage of ordering seen in the Ni^{2+}/Mn^{4+} spinels [16] and tracks well with the Mn^{4+} content inferred from the aforementioned XRD studies.

3.3. Electrochemical characterization

The 1st and 2nd Galvanostatic charge–discharge voltage profiles of the spinels annealed at temperature ranges of 350–900 °C are illustrated in Fig. 7. As shown, the development of Ni^{2+}/Ni^{3+}, Ni^{3+}/Ni^{4+} plateaus belong to Ni redox reactions in the voltage range of 4.75–4.80 V (depending on charge/discharge profile) as well as 4 V plateau belong to Mn^{3+}/Mn^{4+} were observed. The distribution of the capacity at voltages less than 4.5 V decreased when the annealing temperature increased from 350 °C up to 600 °C. Above 600 °C the capacity at 4 V again increased. This is consistent with the maximum amount of Mn^{4+} (minimum Mn^{3+}) being present at 600 °C as the 4 V feature is a direct result of $Mn^{3+} \rightarrow Mn^{4+}$ redox. This is also consistent with the minimum in the lattice parameter observed in the 600–650 °C region as one would expect for a Mn^{4+} rich spinel. The small systematic increase in 4 V plateau above 600 °C parallels the introduction of more Mn^{3+}. This again coincides well with the small increase in lattice parameter observed in this region which can be attributed to the increase in the larger Mn^{3+} content. Finally, it is of interest to note that the double plateau like split at 4.7 V increases with temperature and is nearly flat at in the samples with

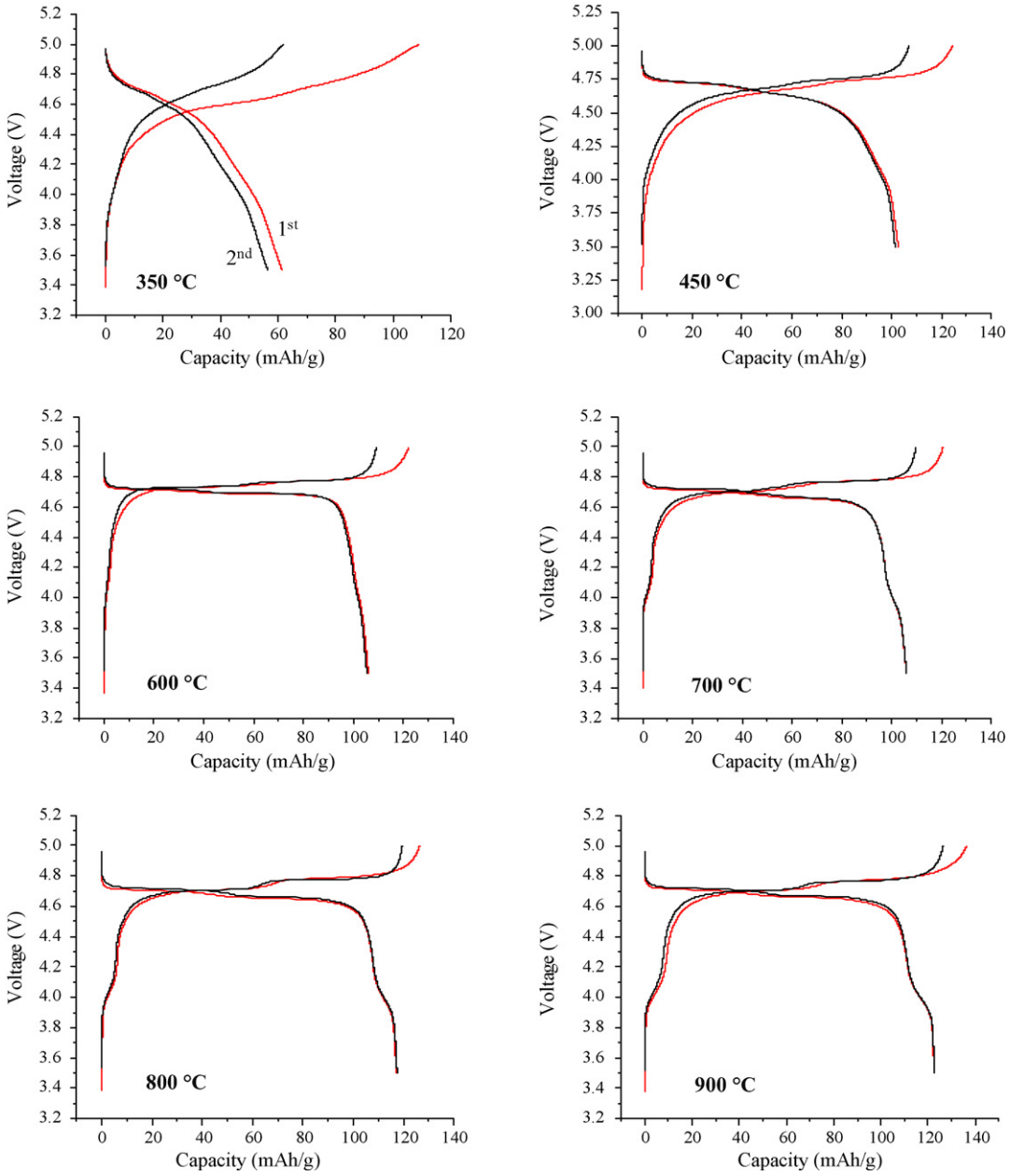

Fig. 7. Galvanostatic charge–discharge profiles of $LiMn_{1.5}Ni_{0.5}O_4$ spinels annealed at different temperatures (350–900 °C) at their initial two cycles. Rate: 44 mA g^{-1}.

the highest Mn^{4+} content. We have shown that the decrease in the split coincides with percentage of $P4_332$. This agrees well with the FTIR which proclaims $P4_332$ dominance in the 600–700 °C range.

Galvanostatic discharge cycling graphs (24 and 60 °C) of the annealed spinels are illustrated in Fig. 8. As shown, the initial discharge capacity increased with annealing temperature in both the 24 and 60 °C cycling conditions. The spinel underwent a 36% and 40% increase in RT and 60 °C discharge capacities, respectively when the anneal temperature was increased from 350 to 450 °C (see Table 1). This is a direct result of the aforementioned lithiation of the spinel and the relocation of the transition metal from the 8a tetrahedral sites to the 16d octahedral. The evolution of structure may have also affected the first cycle irreversible loss showing ~60% decline in value. However, we need to consider the surface area effect on irreversible loss which was decreased at higher temperatures. Analogous to irreversible loss, cycling stability was also improved. Samples annealed at 800 °C showed 3.2% loss after 50 cycles at 60 °C and 900 °C annealed samples exhibited 2.4% loss at 24 °C (Table 1). With respect to 60 °C performance, 800 °C cells with the lowest surface area, demonstrated the highest discharge capacity, the least irreversible loss and the best cycling stability. It is evident that the lower surface area in 800 °C cells was consistent with the lower electrode–electrolyte interface area and hence less side reactions at this interface during the course of 60 °C cycling. The influence of surface area on cycling stability at elevated temperature is discussed in the following section.

3.4. Effect of surface area on electrochemical performance

The effect of cathode surface area on the 60 °C cycling of two different phase pure spinel cathodes prepared by Pechini and solid-state processes, both belong to $Fd\bar{3}m$ space group, were studied and compared in Fig. 9. Pechini-processed powder with lattice parameter of $a = 8.1682$ Å and surface area of 5.5 m^2 g^{-1} was based on wet chemical route which utilized nitrate-based precursors, while the solid-state (SS) process ($a = 8.1845$ Å) with

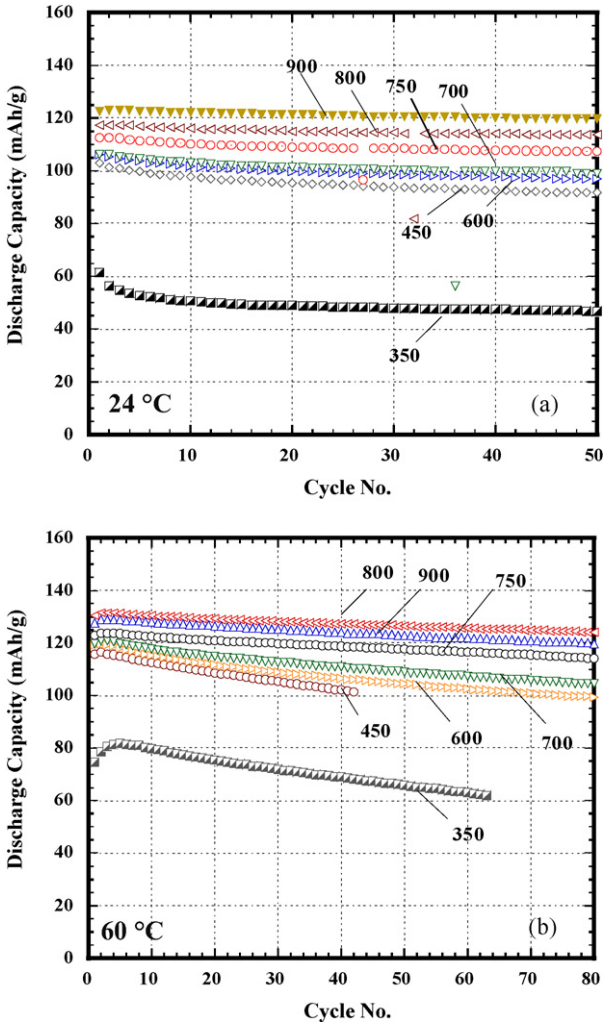

Fig. 8. Effect of different annealing temperatures on (a) 24 °C and (b) 60 °C galvanostatic cycling of $LiMn_{1.5}Ni_{0.5}O_{4-\delta}$ spinel. Rate: 44 mA g^{-1}, Electrolyte: 1 M $LiPF_6$: EC-DMC (1:1, v/v).

oxide-carbonate based precursors had surface area of 1.6 m^2 g^{-1} [16,25,26]. The particle morphology in Pechini was composed of interconnected nano-size particles while the SS powder had relatively discrete well-crystalline particles with smooth (1 1 1) faceted

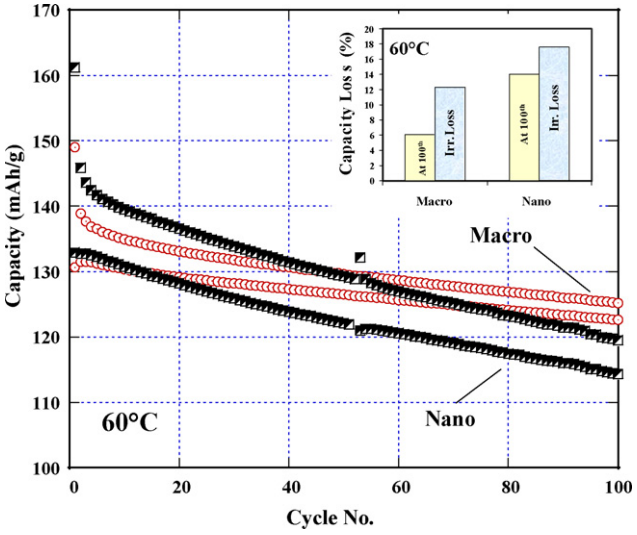

Fig. 9. Effect of surface area on electrochemical performance of $LiMn_{1.5}Ni_{0.5}O_{4-\delta}$ prepared by Pechini (with nanometer particles) and solid-state processes at 60 °C. Rate: 44 mA g^{-1}.

octahedral morphology. As shown in Fig. 9 the cell with the spinel prepared by the Pechini process showed higher initial charge and slightly higher discharge capacities over the SS powder. The irreversible capacity loss was also much higher in Pechini versus SS while the columbic efficiency during cycling showed the opposite trend.

The slightly higher capacity in the spinel prepared by the Pechini process is mainly due to the large surface area (>3 times of SS) cathode which provides large area for Li intercalation/deintercalation. More importantly, this large surface area also provides more electrolyte–cathode contacts which promote interface side reactions especially at elevated temperature and high voltage (i.e. charged state) [27] increasing the degradation and the average impedance of the positive electrode [28]. In general, the thermodynamic stability for most of the electrolytes falls below 4 V, where the cell can utilize the full advantage of the nano-structure morphology, such as higher capacity and improved rate capability. However, in the operating voltage of >4 V, the stability of electrolyte is lowered by catalytic driven surface reactions [29]. By comparing the voltage profiles of nano- and macro-sized spinels at 100th cycle, rapid increase in electrical impedance of the nano-sized spinel (Pechini-processed cell) was observed, whereas, the

Table 1
Summary of physical and electromechanical properties of the $LiMn_{1.5}Ni_{0.5}O_{4-\delta}$ spinel synthesized by two-step process.

Properties	350 °C	450 °C	600 °C	700 °C	750 °C	800 °C	900 °C
Lattice parameter, a (A)	8.2522	8.1883	8.1745	8.1780	8.1782	8.1793	8.1791
Specific surface area, S (m^2 g^{-1})	9.1	7.5	6.0	5.4	4.3	4.4	4.5
Average particle size[a], d (nm)	149.1	179.5	225.4	247.9	315.0	308.6	301.7
First cycle irreversible loss (%)							
24 °C	43.7	17.1	13.8	11.8	11.0	7.5	10.4
60 °C	44.9	25.8	21.7	18.5	15.3	12.3	15.5
Discharge capacity (mAh g^{-1})							
24 °C	61.4	102.7	106.0	106.0	112.5	117.2	122.7
60 °C	74.5	115.9	119.3	119.8	123.0	130.7	127.9
Capacity loss at 50 cycle (%)							
24 °C	23.8%	10.9%	8.6%	6.7%	4.6%	3.1%	2.4%
60 °C	11.7%	–	12.4%	9.1%	4.3%	3.2%	3.8%
Columbic efficiency[b] (%)							
24 °C	96.9%	97.7%	98.6%	98.6%	99.0%	99.2%	99.1%
60 °C	93.6%	93.1%	92.9%	95.0%	95.8%	96.6%	96.2%

[a] Average particle size (d) was estimated based on $d = 6/S \times p$ (S: specific surface area in m^2 g^{-1}, p: density in g cm^{-3}).
[b] Columbic efficiency at cycle 10.

rise in impedance was much smaller for SS. This could indicate the higher extent of electrolyte decomposition (oxidation of electrolyte) and cathode destruction (Mn dissolution in electrolyte) in Pechini versus SS spinel [28]. The rapid impedance growth followed by cell failure in nano-sized (Pechini) and macro-sized (solid-state) spinels was observed at cycle numbers of 110 and 150, respectively, demonstrating the effect of surface area on cycle life.

4. Summary and conclusions

A new solid-state process for synthesis of the $LiMn_{1.5}Ni_{0.5}O_{4-\delta}$ spinel of good electrochemical properties was developed. The process consisted of the formation of $Ni_{0.67}Mn_2O_{4-\delta}$ spinel followed by subsequent Li introduction into the primary spinel structure. This simple process allowed us to obtain the spinel framework starting from temperatures as low as 350 °C. Introduction of Li changed the $Ni_{0.67}Mn_2O_{4-\delta}$ spinel by inducing Ni/Mn ion migrating from partially occupied tetrahedral 8a sites (in $Ni_{0.67}Mn_2O_{4-\delta}$) to the octahedral 16d sites in disordered ($Fd\bar{3}m$) spinel ($LiMn_{1.5}Ni_{0.5}O_{4-\delta}$). The final spinel material demonstrated a good elevated temperature performance with columbic efficiency of ≥97% and discharge capacity retention of ∼94% at 100th cycle at 60 °C.

Acknowledgements

Research was sponsored by the Army Research Laboratory and was accomplished under cooperative agreement number W911NF-06-2-0044. The views and conclusions contained in this document are those of the authors and should not be interpreted as representing the official policies, either expressed or implied, of the Army Research laboratory or the U.S. Government. The U.S. Government is authorized to reproduced and distribute reprints for Government purposes notwithstanding any copyright notation heron.

References

[1] Q. Zhong, A. Bonakdarpour, M. Zhang, Y. Gao, J. Dahn, J. Electrochem. Soc. 144 (1997) 205.
[2] J.-H. Kim, S.-T. Myung, C.S. Yoon, S.G. Kang, Y.-K. Sun, Chem. Mater. 16 (2004) 906.
[3] M.G. Lazarraga, L. Pascual, H. Gadjov, D. Kovacheva, K. Petrov, J.M. Amarilla, R.M. Rojas, M.A. Martin-Luengo, J.M. Rojo, J. Mater. Chem. 14 (2004) 1640.
[4] A. Eftekhari, J. Power Sources 124 (2003) 182.
[5] T. Ohzuku, K. Ariyoshi, S. Takeda, Y. Sakai, Electrochim. Acta 46 (2001) 2327.
[6] H.C. Wang, C.H. Lu, J. Power Sources 119 (2003) 738.
[7] S.H. Wu, H.J. Su, Mater. Chem. Phys. 78 (2002) 189.
[8] H. Kawai, M. Nagata, H. Kageyama, H. Tukamato, A.R. West, Electrochim. Acta 45 (1999) 315.
[9] M.E. Arroyo y de Dompablo, J. Morales, J. Electrochem. Soc. 153 (2006) A2098.
[10] S.-H. Park, S.-W. Oh, S.-T. Myung, Y.-K. Sun, Electrochem. Solid-State Lett. 7 (11) (2004) A451–A454.
[11] M.M. Thackeray, P.J. Johnson, L.A. De Picciotto, P.G. Bruce, J.B. Goodenough, Mater. Res. Bull. 19 (1984) 179.
[12] K. Takahashi, M. Saitoh, M. Sano, M. Fujita, K. Kifune, J. Electrochem. Soc. 151 (1) (2004) A173–A177.
[13] S. Wu, S. Kim, J. Power Sources 109 (2002) 53–57.
[14] S.L. Swartz, T.R. Shrout, Mater. Res. Bull. 17 (1982) 1245.
[15] S.L. Swartz, T.R. Shrout, W.A. Schulze, L.E. Cross, J. Am. Ceram. Soc. 67 (5) (1984) 311–315.
[16] M. Kunduraci, G.G. Amatucci, J. Electrochem. Soc. 153 (7) (2006) A1345–A1352.
[17] D.G. Wickham, "Preparation of $NiMnO_3$", US Patent 3,380,919 (1968).
[18] X. Tang, A. Manthiram, J.B. Goodenough, J. Less-Common Met. 156 (1989) 357–368.
[19] E.D. Macklen, Thermistors, Electrochemical Publication Ltd, UK, 1979.
[20] E.D. Macklen, J. Phys. Chem. Solids 47 (1986) 1073.
[21] R. Legros, R. Metz, A. Rousset, J. Mater. Sci. 25 (1990) 4410–4414.
[22] K. Ariyoshi, Y. Iwakoshi, N. Nakayama, T. Ohzuku, J. Electrochem. Soc. 151 (2) (2004) A296–A303.
[23] Y. Idemoto, H. Narai, N. Koura, J. Power Sources 119–121 (2003) 125–129.
[24] M. Kunduraci, G.G. Amatucci, J. Power Sources 165 (2007) 359–367.
[25] M.P. Pechini, U.S. Patent, 3,330,697 (1967).
[26] W. Liu, G.C. Farrington, F. Chaput, B. Dahn, J. Electrochem. Soc. 143 (1996) 879–884.
[27] G.G. Amatucci, C.N. Schmutz, A. Blyr, C. Sigala, A.S. Gozdz, D. Larcher, J. Power Sources 69 (1997) 11–25.
[28] N. Marandian Hagh, Sylvie Rangan, Frederic Cosandey, Robert Bartynski, G.G. Amatucci, J. Electrochemical Society 157 (3) (2010) A305–A319.
[29] G.G. Amatucci, J.-M. Tarascon, J. Electrochem. Soc. 149 (12) (2002) K31–K46.